



HAL
open science

Noncontact Layer Stabilization of Azafullerene Radicals: Route toward High-Spin-Density Surfaces

Yuri Tanuma, Gregor Kladnik, Luca Schio, Marion van Midden Mavrič,
Bastien Anézo, Erik Zupanič, Gregor Bavdek, Ruben Canton-Vitoria, Luca
Floreano, Nikos Tagmatarchis, et al.

► To cite this version:

Yuri Tanuma, Gregor Kladnik, Luca Schio, Marion van Midden Mavrič, Bastien Anézo, et al.. Non-contact Layer Stabilization of Azafullerene Radicals: Route toward High-Spin-Density Surfaces. ACS Nano, 2023, 17 (24), pp.25301-25310. 10.1021/acsnano.3c08717 . hal-04423709

HAL Id: hal-04423709

<https://hal.science/hal-04423709>

Submitted on 29 Jan 2024

HAL is a multi-disciplinary open access archive for the deposit and dissemination of scientific research documents, whether they are published or not. The documents may come from teaching and research institutions in France or abroad, or from public or private research centers.

L'archive ouverte pluridisciplinaire **HAL**, est destinée au dépôt et à la diffusion de documents scientifiques de niveau recherche, publiés ou non, émanant des établissements d'enseignement et de recherche français ou étrangers, des laboratoires publics ou privés.

Non-contact layer stabilization of azafullerene radicals: route towards high-spin-density surfaces

Yuri Tanuma^{1,2#§}, Gregor Kladnik^{3,4§}, Luca Schio⁴, Marion van Midden Mavrič¹, Bastien Anézo⁵, Erik Zupanič¹, Gregor Bavdek^{4,6}, Ruben Canton-Vitoria⁷, Luca Floreano⁴, Nikos Tagmatarchis⁷, Hermann A. Wegner^{8,9}, Alberto Morgante^{4,10}, Chris Ewels^{5}, Dean Cvetko^{1,3,4*}, Denis Arčon^{1,3*}*

¹ Jožef Stefan Institute, Jamova 39, SI-1000, Ljubljana, Slovenia.

² Center for Advanced Research of Energy and Materials (CAREM), Hokkaido University, Kita 13, Nishi 8, Kitaku, Sapporo 060-8628, Japan.

³ Faculty of Mathematics and Physics, University of Ljubljana, Jadranska 19, SI-1000, Ljubljana, Slovenia.

⁴ CNR-IOM, Istituto Officina dei Materiali, Basovizza Area Science Park, I-34149, Trieste, Italy.

⁵ Institut des Matériaux de Nantes Jean Rouxel (IMN), UMR 6502 CNRS, Nantes University, 44322 Nantes, France.

⁶ Faculty of Education, University of Ljubljana, Kardeljeva ploščad 16, SI-1000 Ljubljana Slovenia.

⁷ Theoretical and Physical Chemistry Institute, National Hellenic Research Foundation, 48 Vassileos Constantinou Avenue, Athens 11635, Greece.

⁸ Institute of Organic Chemistry, Justus Liebig University Giessen, Heinrich-Buff-Ring 17, 35392 Giessen, Germany.

⁹ Center for Materials research (ZfM/LaMa), Justus Liebig University Giessen, Heinrich-Buff-Ring 16, 35392 Giessen, Germany.

¹⁰ Physics department, University of Trieste, Via Valerio 2, 34012, Trieste, Italy.

§ Y.T. and G.K. contributed equally to this work.

Keywords: azafullerene, radicals, qubit, scanning tunnelling microscopy, near edge X-ray absorption fine structure spectroscopy, density functional calculation

Abstract

We deposit azafullerene C₅₉N• radicals in vacuum on Au(111) surface for layer thicknesses between 0.35-2.1 monolayers (ML). The layers are characterized using X-ray photoemission (XPS) and X-ray absorption fine structure (NEXAFS) spectroscopy, low-temperature scanning tunneling microscopy (STM) and by density functional calculations (DFT). The singly unoccupied C₅₉N orbital (SUMO) has been identified in the N 1s NEXAFS/XPS spectra of C₅₉N layers as the spectroscopic fingerprint of the molecular radical state. At low molecular coverages (up to 1 ML), films of monomeric C₅₉N are stabilized with the non-bonded carbon orbital neighboring the nitrogen oriented towards the Au substrate, whereas in-plane intermolecular coupling into diamagnetic (C₅₉N)₂ dimers takes over towards the completion of the 2nd layer. By following the C₅₉N• SUMO peak intensity with increasing molecular

coverage, we identify a novel intermediate high-spin-density phase between 1 and 2 ML, where uncoupled $C_{59}N^{\bullet}$ monomers in the 2nd layer with pronounced radical character are formed. We argue that the $C_{59}N^{\bullet}$ radical stabilization of this supramonolayer phase of monomers is achieved by suppressed coupling to the substrate. This results from molecular isolation on top of the passivating azafullerene contact layer, which opens further ideas for molecular radical state stabilization and positioning on solid substrates.

Introduction

Organic radicals – organic compounds possessing one or more unpaired electrons in their electronic ground state – are usually thought of as transient or unstable species, since their unpaired electrons are highly reactive. However, their stability can be significantly improved by either sterically protecting the unpaired electron sites (for example with bulky side groups), or by increasing the delocalization of the unpaired electrons over several atoms.¹ Such stable molecular radicals are, for example, considered as a simple platform to encode bits in the limits of quantum physics (qubits)² or are a potential route for the design of novel synthetic and catalytic processes.³ One candidate for robust organic molecular radicals is azafullerene $C_{59}N$,⁴ where one nitrogen replaces a carbon atom in the fullerene skeleton. Due to valence inequality between N and C, $C_{59}N$ is a closed-cage hetero-fullerene radical, where the odd electron resides on the carbon neighboring the substitutional nitrogen.⁵ However, due to their high reactivity, it readily forms closed shell dimers $(C_{59}N)_2$ ⁵ or $C_{59}HN$ ⁶ in the bulk phase. The spin-active radical species can then be accessed by thermolysis or photolysis of the parent $(C_{59}N)_2$ ^{7–11} as the two $C_{59}N$ units are weakly bound by ~ 0.78 eV, but they nevertheless show high reactivity to ultra-rapid re-dimerization (under inert conditions) or oxidation (in ambient environment).

From the perspective of molecular qubit applications, any complex architecture of molecular qubits needs to be ultimately placed in some 2D network, and molecular spin

manipulation on solid substrates appears to be the next necessary step.¹² The stability of molecular spins then decisively relies on particular interaction with the surface and suppressed intermolecular coupling that prevents formation of non-magnetic oligomer or polymer assemblies. Similar requirements may be defined also for the radical catalytic reactions. Multilayers of azafullerenes on solid substrates have been previously realized in ultra-high vacuum (UHV) by thermal deposition of $C_{59}N^{\bullet}$ monomers, but the formed layers have been found predominantly in their stable diamagnetic $(C_{59}N)_2$ dimer entities.¹³ Early studies of $C_{59}N^{\bullet}$ on reactive Si(111)-(7x7) and Si(100)-(1x2) surfaces indicate that almost no dimerization takes place at submonolayer coverage, proving that azafullerene sublimes as $C_{59}N^{\bullet}$ monomers by UHV thermal deposition, yet no direct spectroscopic evidence of the radical character of such monomers on Si was given.^{14–16}

Similarly, $C_{59}N^{\bullet}$ monomer stabilization was reported for azafullerene monolayers on Cu(111), where strong binding to the substrate was observed.¹⁷ In fact, significant charge transfer from Cu to $C_{59}N^{\bullet}$ was reported for the contact layer,¹⁷ which stabilizes monomers over dimers on Cu(111) and at the same time completely quenches the radical character of the azafullerene monomers.

The choice of Au(111) is expected to provide a substrate with sufficiently weak interaction to avoid covalent bonding with $C_{59}N^{\bullet}$ and thus preserve the radical state of azafullerenes. In fact, for a similar organic system – 1,2,4-benzotriazin-4-yl radical (Blatter radical) – the radical character of single Blatter molecules could be retained on Au(111), as proven by near edge X-ray absorption fine structure (NEXAFS) spectroscopy¹⁸ and scanning tunneling microscopy (STM) identification of Kondo resonance.¹⁹

Here, we present a comprehensive experimental and theoretical study of ultrathin azafullerene films deposited in UHV on Au(111) surface. From X-ray photoemission (XPS)

and NEXAFS spectroscopy we determine the azafullerene coupling and the radical state in films up to 2 monolayers (ML) thickness. Supported by DFT results, we find the direct spectroscopic fingerprint of the $C_{59}N^{\bullet}$ radical state in the nitrogen K-edge NEXAFS, as the occurrence of a singly unoccupied molecular orbital (SUMO) lying close to the Fermi level. Analysis of NEXAFS and the complementary low-temperature topographic STM images prove that initially $C_{59}N^{\bullet}$ monomers form hexagonally packed islands where individual azafullerenes orient towards the Au(111) surface with their non-bonded carbon orbital neighboring the nitrogen. The radical character of $C_{59}N^{\bullet}$ monomer films is elucidated from the analysis of NEXAFS and shake-up structures in the N 1s XPS peak, i.e., photoelectron energy losses due to highest occupied molecular orbital (HOMO) to lowest unoccupied molecular orbital (LUMO) excitations. Site selective charge transfer between $C_{59}N^{\bullet}$ monomers and Au substrate is found for the monolayer films as the contact strength between monomers and Au substrate varies within the azafullerene islands due to their lattice mismatch with Au(111). Finally, we discover a novel high-density radical phase for the $C_{59}N^{\bullet}$ supramonolayer (ML+) phase at coverage between 1-2 ML, where $C_{59}N^{\bullet}$ monomers are isolated on top of the 1st layer. These molecules exhibit the largest SUMO peak intensity in the NEXAFS spectra and give insight in the nature of efficient stabilization of molecular radicals and their spins.

Results and Discussion

Topographic STM images of deposited $C_{59}N$ material on Au(111) surface reveal two-dimensional islands of hexagonally packed azafullerenes that start to grow at the step edges of the Au substrate (Fig.1a). These islands are orientationally commensurate with the Au(111) with close packed rows of molecules aligned with the rows of Au surface atoms running along [0-11], [-110], and [10-1], respectively. A line profile along [0-11] has a height difference of

~6-8 Å with the substrate (Fig. 1b) showing that the observed island of C₅₉N is a monolayer. Measured average center-to-center ball distances along the three different principal directions are 10.2 Å, 10.4 Å, and 10.3 Å (Fig. 1b, Fig.S1b), respectively. These distances are considerably longer compared to the (C₅₉N)₂ intradimer center-to-center distance of 9.41 Å and are comparable to interdimer center-to-center distances of 9.81 Å and 10.11 Å in (C₅₉N)₂ solid.²⁰ This suggests that the interaction between the electron in the frontier molecular orbital with the Au surface and π - π interaction between azafullerenes defines the hexagonal packing of the islands as well as their relative orientation.

The interaction of adsorbed C₅₉N with the Au(111) most likely proceeds with the C₅₉N• non-bonded carbon orbital neighboring the nitrogen that is oriented towards the Au surface. Our NEXAFS experiments as well as DFT calculations presented below indeed confirm this. Interestingly, careful examination of low-temperature STM images suggest that C₅₉N• bonded to the substrate are not uniformly adsorbed at the same orientation, nor at a uniform height from Au surface (insets to Fig. 1a). The difference in the Au–C contact angle measured against the normal to the Au surface (Fig. 1c) results in at least two different orbital shapes, holding a 3-fold and 2-fold symmetry, when observed from the top. The orbital shape with a 2-fold symmetry corresponds to the C₅₉N orientation with the hexagon-hexagon bond at the top (6:6-top, inset to Fig. 1a). On the other hand, the 3-fold symmetry of the molecular orbital is approximately reproduced in cases when the azafullerene slightly tilts bringing the vortex between the two hexagons and the pentagon to the apex (5:6-top) or when the displacement of the azafullerene is even larger bringing hexagon to the top (hex-top, inset to Fig. 1a and Fig. 1c). We stress that some tilting of the C₅₉N monomers is necessary in order to accommodate adsorbed molecules to the Au(111) lattice. Similar orbital shape patterns were previously observed also for the C₆₀ monolayer films on an Au(111) substrate.²¹

DFT calculations of a C₅₉N monolayer on Au(111) confirm that there is an energetic preference for the azafullerene to orient with the carbon dangling bond towards an Au-atom in the layer below, at an Au-C distance of 2.22 Å (Fig. S2). This puts the nitrogen atom at a 27° angle from the surface normal. Rotating the C₅₉N about its center of mass in a series of single-point energy calculations shows the binding rapidly drops with angle, reaching >0.5 eV less stable for rotations above 15° (Fig. S2). This suggests **monomers** will only be surface oriented with relatively small angular variation, in agreement with STM observation.

In contrast to the case of C₅₉N adsorbed on Cu(111),¹⁷ Mulliken population analysis suggests weak charge transfer to the substrate (~0.10e per cage). However, projected density of states (Fig. S3) shows the azafullerene states near the Fermi level are strongly dispersed, indicating strong mixing with gold and as such Mulliken estimates are likely to be inaccurate.

We next calculated C₅₉N at 25% surface coverage (4x4 Au supercell). Comparing to isolated gas-phase C₅₉N gives a binding enthalpy of 1.216 eV per C₅₉N to pristine flat Au(111). This rises to 2.837 eV when the C₅₉N are in the 100% monolayer, clearly showing the driving force for close packing as seen in STM. Repeating these calculations without Au present shows that 0.567 eV of this increase in binding comes from interaction between neighboring fullerenes in the monolayer. This does not, however, account for all of the binding increase calculated upon azafullerene close-packing. This suggests therefore that close packing must also increase Au-C₅₉N interaction. Adding a second monolayer of C₅₉N*, the binding energy per C₅₉N* in this layer decreases to 1.392 eV, around the half in comparison with the first monolayer, confirming a strong thermodynamic drive to form complete monolayer surface coverage of Au before C₅₉N will deposit on top. This is also consistent with the STM data where close-packed surface monolayers form in preference to three-dimensional island clusters, and corroborates again the strong Au-C₅₉N* interaction.

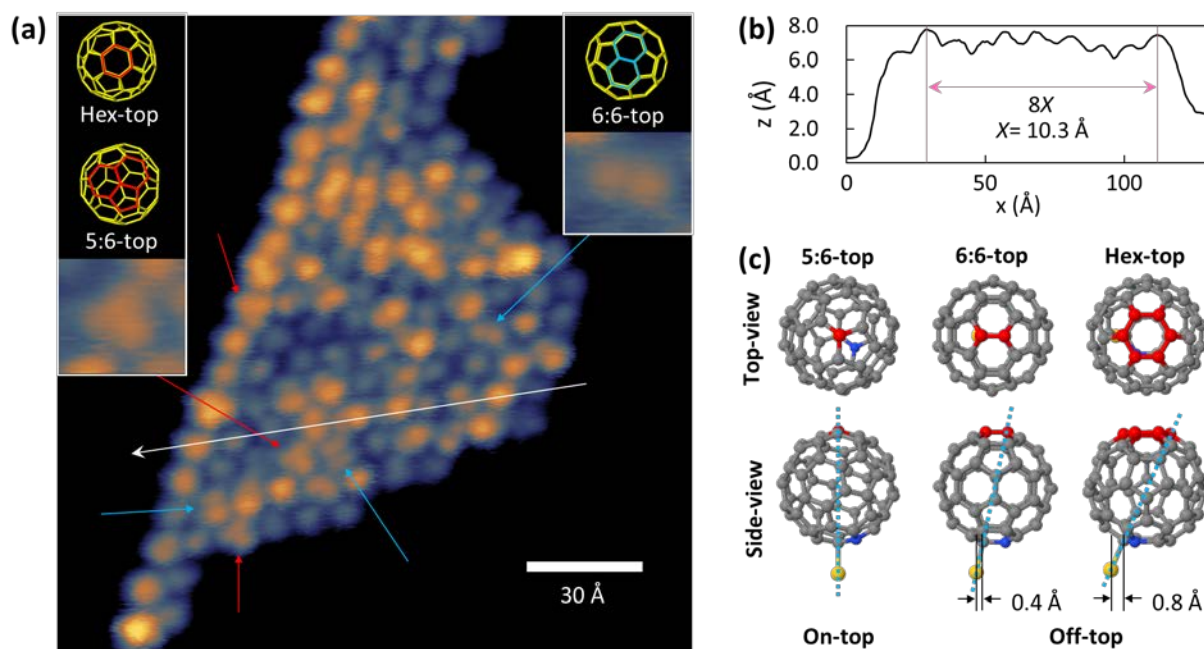


Figure 1. (a) STM image of $C_{59}N$ island formed on Au(111) substrate taken by 100 pA tunneling current and 500 mV bias voltage. Red and blue arrows are pointing orbitals of 3-fold (5:6- or hex-top $C_{59}N$, left inset) and 2-fold (6:6-top $C_{59}N$, right inset) symmetries, respectively. White arrow shows the direction of [0-11] and is the cross-section used for x-z analysis (b). (c) When $C_{59}N$ shifts away from the position exactly above the Au atom in the substrate layer (side-view), the top view of the molecule changes from the approximately 3-fold to 2-fold and back to 3-fold symmetry (top). Grey, red, blue and yellow balls represent atoms of C, C at the top, N and Au, respectively. Dashed cyan line shows the tilting of azafullerene.

The STM and DFT results demonstrate considerable interaction between the adsorbed $C_{59}N^{\bullet}$ and the Au(111) surface within the 1st monolayer, but do not provide a clear insight into the radical state of the $C_{59}N$ entities. We thus next turn to X-ray spectroscopy. In Fig. 2a we compare the C 1s and N 1s photoemission peaks for 10 Å and 17 Å thickness azafullerene films on Au(111). For the 17 Å film thickness, the 1s core levels of C and N are observed at binding energies of 285.0 eV and 400.6 eV, respectively, in agreement with the values for thick $(C_{59}N)_2$ films reported in the literature.^{13,22} Relative to these two reference binding energies, the C 1s

and N 1s peaks are systematically shifted to lower binding energies by about 0.25 eV and 0.35 eV for film thicknesses up to 8 Å (inset to Fig. 2a), respectively. This energy shift is attributed to core-hole screening by the Au(111) surface and predominantly applies to the molecules closest to the Au surface, i.e., molecules within the 1st monolayer. The change of binding energy observed beyond 8 Å can be associated with the crossover from the 1st to 2nd layer where core-hole screening by the Au substrate is suppressed. The relative sharpness of the binding energy change indicates that C₅₉N initially uniformly covers the Au(111) surface up to 1 ML (8 Å) before the 2nd layer growth sets-in, just as observed by STM (Fig. 1a) and DFT calculations. We also note that the N 1s XPS peak displays a constant peak profile throughout the 0-8 Å coverage range without significant broadening, indicating that the distribution of C₅₉N-Au contacts remains nearly the same throughout the monolayer coverage range. In fact, any significant reorientation of the N within the fullerene cage in the 1st layer would introduce a different spread of binding energy shifts due to Au screening, which is not observed. We finally note that XPS spectra does not change within the experimental time of several hours implying that C₅₉N films are very stable under inert conditions for all coverage thicknesses.

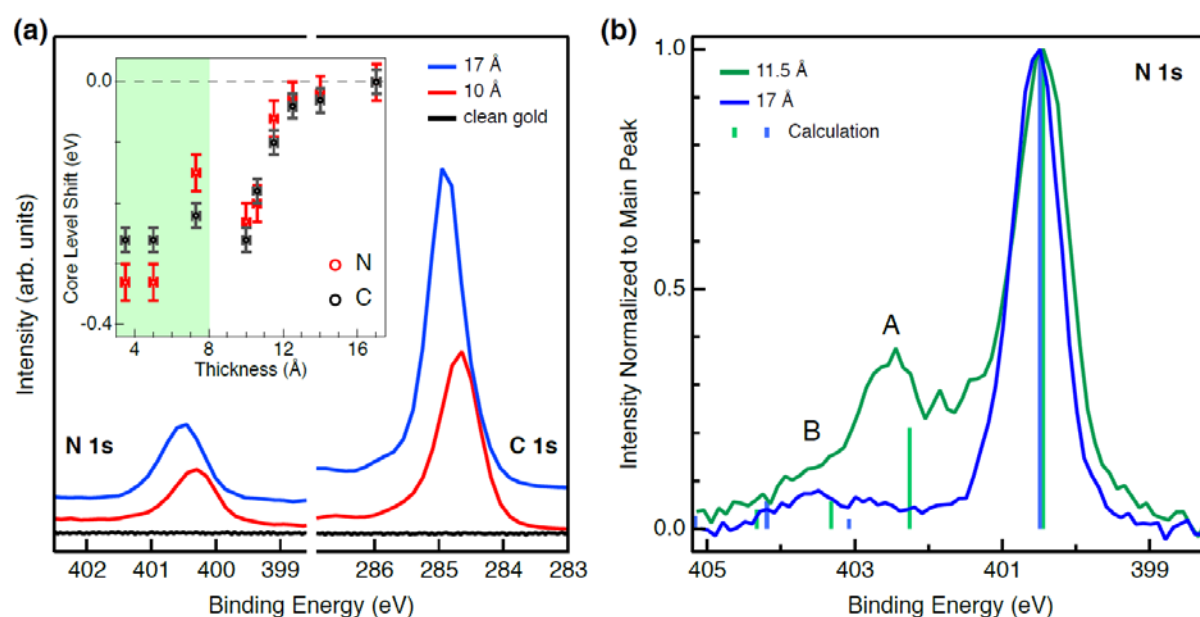


Figure 2. (a) XPS of C 1s, N 1s measured for 10 Å deposited C₅₉N film (~1.2 ML red curve) and for 17 Å film (~2.1 ML, blue curve). Inset: the C 1s and N 1s screening shift with respect to the Au(111) for increasing coverage. Crossover from 1st to 2nd layers is indicated at 8 Å by the green-white shading boundary. (b) XPS N 1s shake-up spectrum for 11.5 Å (green line) and 17 Å (blue line) thick layers of C₅₉N/Au(111). Theoretically calculated peaks for (C₅₉N)₂ dimer and C₅₉N• monomer taken from ref.23 are marked with green and blue vertical lines, respectively. The spectrum of 11.5 Å thick layer (green) shows a prominent satellite peak at 402.3 eV (feature A) and a smaller satellite peak at 403.1 eV (feature B) which qualitatively match with the calculated satellite peaks for the radical monomer, whereas the spectrum of 17 Å (blue) displays two peaks at 402.7 and 403.5 eV that match closely the calculated satellite peaks for the (C₅₉N)₂ dimer.

The electronic nature of the adsorbed C₅₉N• may be further understood from analysis of the shake-up satellites of the C 1s and N 1s XPS peaks. In the C 1s shake-up spectrum of C₅₉N• films on Au(111) we observe a shoulder in the high energy tail of the C 1s peak at around ~1 eV from the main elastic line (Fig. S4). The energy difference between the elastic line and the shake-up satellite (photoelectron energy loss) corresponds to electron excitation from the occupied to unoccupied states (*e.g.*, HOMO to LUMO) and has been previously observed in bulk films of (C₅₉N)₂ but not for C₆₀ films. Therefore, it can be related to the sp³ carbon next to N in the azafullerene cage, which in monolayers bonds to the Au and in multilayer films crosslinks to form a dimer.²²

However, according to the calculated C 1s shake-up excitations for different C₅₉N derivatives^{23,24}, the C 1s shake-up peaks are not sensitive to the radical state of the azafullerene films (Fig. S4). We thus rather turn to the shake-up satellites of the N 1s XPS peak (Fig. 2b)

where we observe a noticeable difference between the films of 11.5 Å and 17 Å film thickness (~1.4 ML and ~2.1 ML, respectively). For the ~2.1 ML film a faint peak (A) shifted by ~2.2 eV and a second peak (B) by ~3.1 eV from the main elastic peak are measured. On the other hand, the shake-up spectrum for 1.4 ML sample shows a pronounced peak centered at ~1.8 eV from the N 1s main line. The nature of these loss peaks can be explored with the help of theoretical calculations for the C₅₉N• monomer and (C₅₉N)₂ dimer structures.²³ The calculated positions of A and B peaks and the overall shape of the loss structure for the (C₅₉N)₂ dimer agrees well with our spectrum for the film-thickness of 17 Å, confirming that C₅₉N• forms dimers at 2.1 ML. This is also in agreement with the previous report for the azafullerene multilayer films.^{13,14} In contrast, the N 1s shake-up spectrum of 11.5 Å film closely resembles the calculated shake-up structure for the C₅₉N• monomers in their radical state. In particular, the loss peak at ~402.3 eV binding energy, which matches the calculated position and relative intensity, is exclusively predicted for the C₅₉N• monomer, but not for other candidate species like (C₅₉N)₂ dimers. Both the shift and the relative increase in intensity of this peak are consistent with the radical character of C₅₉N• monomers in the monolayer. Namely, the radical orbital, although primarily centered on the C site neighboring N, exhibits significant overlap with the nitrogen.²³ This overlap is for example also evidenced by the characteristic hyperfine splitting in the EPR spectra of C₅₉N• radicals.^{7–9} So, we conclude that the measured shake-up structure of C₅₉N• monomers reflects their radical state (Fig. 2b).

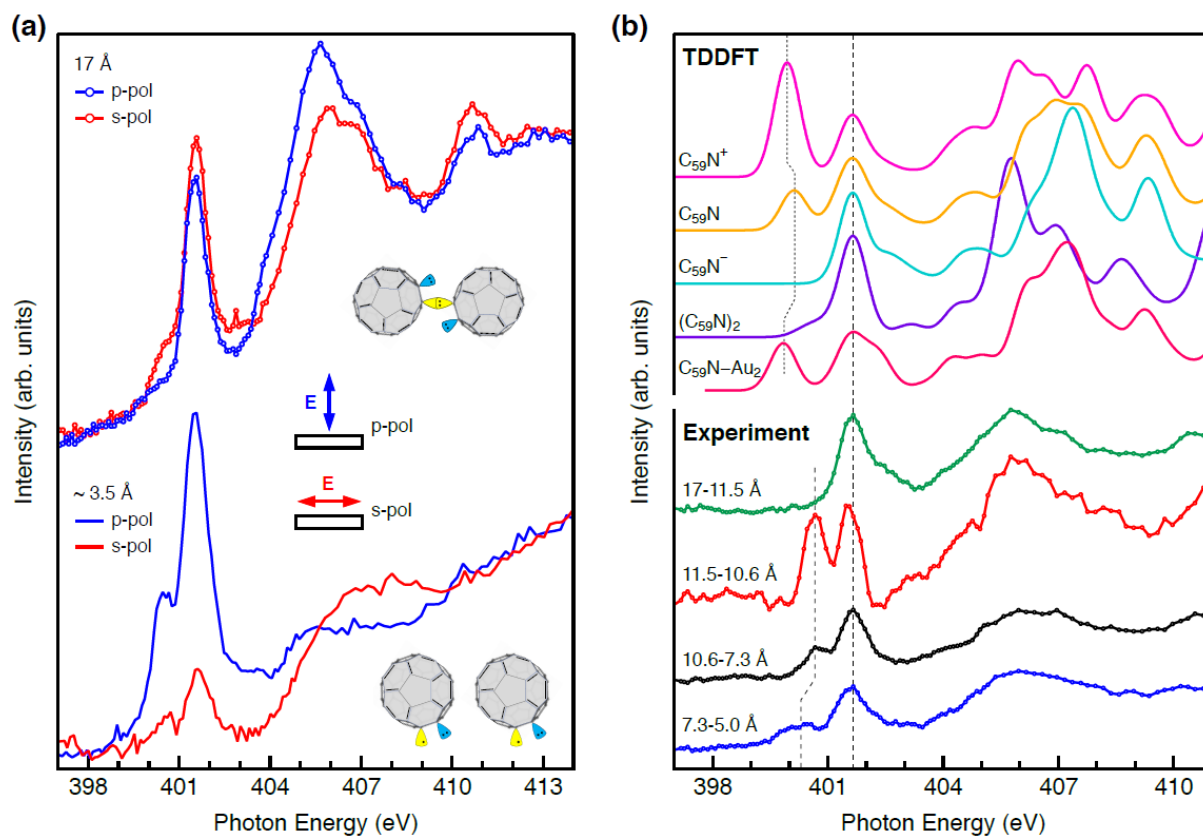


Figure 3. (a) N K-edge NEXAFS linear dichroism for 3.5 Å thick film C₅₉N (lower panel) and 17 Å thick film (upper panel). The average orientation of the N site of the azafullerene cage is indicated in the insets. (b) Layer resolved sequence of differential NEXAFS in “magic” superposition of p-polarization and s-polarization spectra are compared with the calculated ones for the (C₅₉N)₂, C₅₉N⁻, C₅₉N[•], C₅₉N⁺ molecules and the artificial C₅₉N–Au₂ complex with 2.0 Å coupling distance, respectively. For the calculated spectra we used time-dependent DFT (TDDFT) calculations (see Methods for details). All spectra are intensity scaled to the probed coverage, and offset vertically for clarity.

We now turn to the NEXAFS spectra. Both, C 1s and N 1s NEXAFS for the 17 Å (~2.1 ML) C₅₉N film (Fig. 3a and Fig. S5a) closely resemble those reported earlier for (C₅₉N)₂ thick films.^{13,22} The principal peaks are due to the transitions from core level to the LUMO and above. We note that the C 1s → LUMO (LUMO+1) resonance at the photon energy $h\nu = 284.9$

eV (286 eV) aligns with the N 1s \rightarrow LUMO (LUMO+1) resonance at 400.7 eV (401.6 eV), see Fig. S5b. The same alignment has been previously reported also for (C₅₉N)₂ bulk films.^{13,22} The N 1s \rightarrow LUMO peak at 400.7 eV shows up only as a shoulder, indicating a weak LUMO resonance with the N 1s core level (Fig. 3).

Next, we compare the N 1s NEXAFS spectra for 3.5 Å (0.4 ML) and 17 Å (2.1 ML) films. The spectra shown in Fig. 3a have been taken with the photon polarization along the surface normal (p-polarization) and parallel to the surface (s-polarization). The pronounced linear dichroism of the main absorption lines (π^* symmetry resonances) at 3.5 Å indicates that molecules of the 1st layer adopt a rather uniform adsorption configuration with N site of the azafullerene cage oriented towards the substrate at $30\pm 3^\circ$ average angle from the surface (inset to Fig. 3a). This is in excellent agreement with the low-temperature STM experiments and DFT computations discussed above (Fig. 1 and Fig. S2) and experimentally demonstrates that C₅₉N• indeed couples to Au(111) via the cage orbitals on carbon next to the substitutional nitrogen atom.

Interestingly, the N 1s NEXAFS spectra taken with the same photon polarizations on 17 Å film with two completed layers of C₅₉N• lack this strong dichroism indicating that the 2nd layer adopts very different geometry (Fig. 3a). Instead, the intensity of these N π^* resonances in s-polarization even exceeds that of p-polarization, pointing to an average orientation of nitrogen atoms in the completed 2nd layer close to 60° from the surface. This agrees well with (C₅₉N)₂ dimer formation of the 2nd layer molecules with C-C bond oriented in-plane and thus with N orbitals oriented predominantly at $\sim 60^\circ$ from the surface.

In order to follow the evolution from the radical monolayer to the second layer of (C₅₉N)₂ dimers, we next perform differential N 1s NEXAFS analysis by sequentially subtracting spectra taken with increasing coverage (Fig. 3b). In total, five films in the thickness

range between 5-17 Å have been investigated. All spectra have been taken in two orthogonal polarizations (s- and p-polarization) and then added by a linear combination ($p + 2s$) into a synthetic spectrum corresponding to the magic angle. Such “magic” spectral representation has the advantage of being independent of molecular orientation, which as we have just argued, changes with coverage, and therefore reflects only the orbital structure of the added film. Fig. 3b shows the resulting sequence of four “magic” NEXAFS spectra resolved in thickness: (7.3 Å–5 Å), (10.5 Å–7.3 Å), (11.5 Å–10.5 Å) and (17 Å–11.5 Å), respectively. The spectra show a strong variation especially in the low energy absorption line at ~400.5 eV. This peak displays the largest intensity for the supramonolayer coverage (11.5 Å–10.5 Å), whereas it is completely quenched for the (17 Å–11.5 Å) when the coverage approaches the completion of the 2nd layer. The sub-monolayer film (7.3 Å–5 Å) displays only moderate intensity of the 400.5 eV peak and even a small shift (~0.3 eV) to lower energies.

The observed evolution of differential N 1s NEXAFS spectra can be corroborated with DFT calculations of N 1s NEXAFS spectra for the (C₅₉N)₂ dimer and neutral and charged C₅₉N monomers (Fig. 3b). Calculated N 1s NEXAFS spectrum for the (C₅₉N)₂ dimer yields excellent agreement with the experimental (17 Å–11.5 Å) spectrum, confirming dimer formation at the completion of 2nd layer. A close inspection of DFT results reveals that the LUMO of (C₅₉N)₂ is mainly delocalized across the carbon sites with minimal overlap with the N sites.²² This agrees with the observed low intensity of the N 1s → LUMO peak at 400.7 eV measured in the ~2 ML films. Considering instead the C₅₉N[•] monomer, our DFT calculations show that the LUMO of the monomer now spreads also over N (see also Ref. 10). This indicates that the LUMO orbital of the dimer turns into SUMO for the monomer, which also agrees with the observed intensity increase of the lowest energy peak at 400.7 eV in the NEXAFS for the monomer films.

When adsorbed on Au, the $C_{59}N^{\bullet}$ monomer will align its SUMO/SOMO (SOMO=singly occupied molecular orbital) energy to the Fermi level, opening the possibility of charge transfer with the substrate. From our DFT calculations we observe that the dangling radical is a half-filled electronic state at the Fermi level. Removing further charge empties this state and causes a downshift in its energy. In contrast, adding a second electron completely fills the state and hence quenches its signal in NEXAFS (Fig. 3b). The N 1s NEXAFS peak at ~400-401 eV can therefore be attributed to the N 1s excitation to the LUMO/SUMO level, depending on the occupancy of this level, *i.e.*, charge state. The energy position and relative intensity of the N 1s NEXAFS peak at ~400-401 eV is therefore a very sensitive probe of the LUMO/SUMO orbital population of the $C_{59}N$ radical state. To corroborate this finding, we finally computed NEXAFS spectra for artificial $C_{59}N$ -Au₂ complexes to emulate the interaction between adsorbed $C_{59}N^{\bullet}$ and Au substrate. Computations were performed for different C-Au bond lengths ranging from 2 Å to 4 Å (Fig. S6). We report here results with Au-Au distance fixed at 2.6 Å. For the largest C-Au distance of 4 Å, the $C_{59}N$ -Au₂ interaction is weak and thus its N 1s NEXAFS spectrum resembles that of the $C_{59}N^{\bullet}$ in gas phase. On the other hand, as soon as carbon of $C_{59}N$ approaches Au at distances smaller than 3 Å, we notice a systematic shift of the SUMO peak to lower energies. Therefore, increasing the interaction between $C_{59}N^{\bullet}$ and Au results in the increase of SUMO-LUMO splitting. These additional calculations thus finally explain the fine variations in the differential N 1s NEXAS spectra. For the (7.3 Å–5.0 Å) spectrum the first layer of $C_{59}N^{\bullet}$ interacts with the Au surface and thus the SUMO splitting is larger than for the (11.5 Å–10.5 Å) spectrum where the second layer of $C_{59}N^{\bullet}$ is already distanced from the Au surface and thus the interaction with the substrate is negligible.

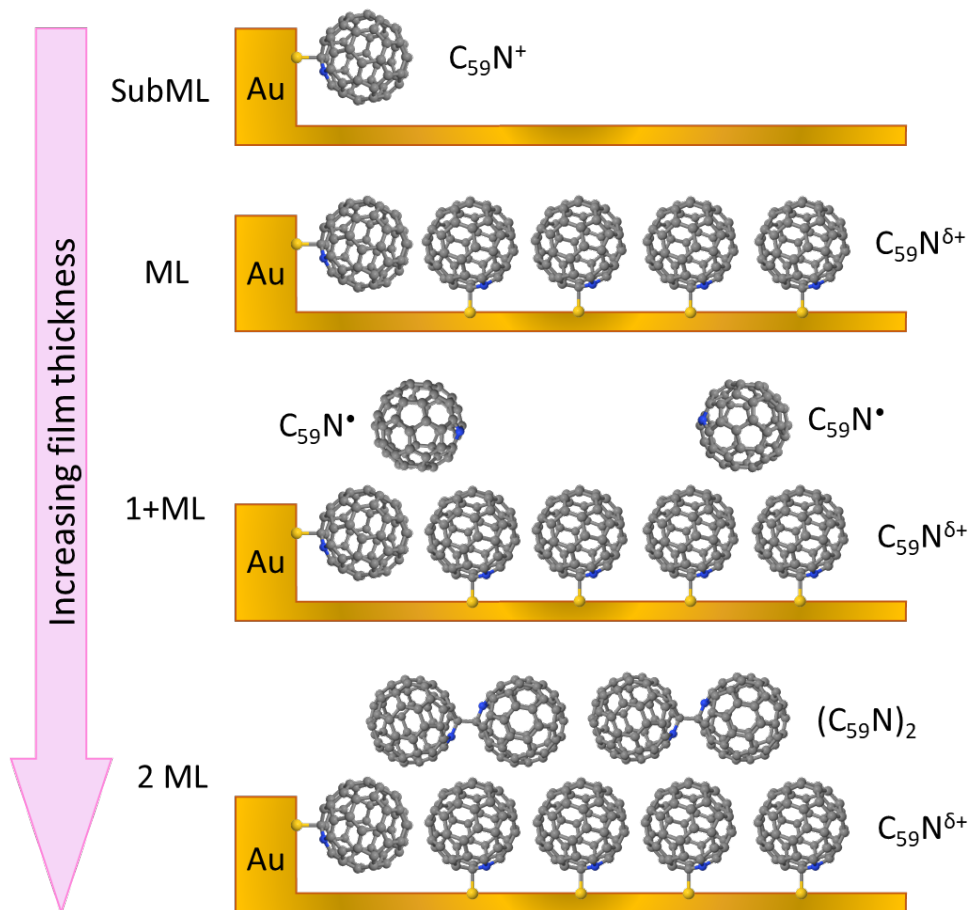


Figure 4. Evolution of C₅₉N[•] radical character as a function of azafullerene film thickness on Au(111). Grey, blue, and yellow spheres represent C, N, and Au atoms, respectively.

We can now build a complete picture of C₅₉N[•] radical state evolution as the thickness of film on Au(111) surface increases (Fig. 4). At very low C₅₉N coverage, *e.g.* (7.3 Å–5 Å), the differential N 1s NEXAFS spectrum, shows a broad SUMO peak around ~400 eV indicating different charge states of the adsorbed species. This is due to partial quenching of the radical character of selected C₅₉N[•] monomers, induced by site dependent C₅₉N-Au coupling and possibly accompanied by a partial charge transfer (see section SA in supplementary information for an extended discussion of the C₅₉N radical state within the 1st monolayer). The coupling to the surface may be particularly favored at Au sites with reduced coordination, such as step edges, where molecules preferentially adsorb as observed by the STM.

Addition of $C_{59}N^{\bullet}$ monomers promotes the growth of the hexagonally packed islands of $C_{59}N^{\bullet}$ monomers that orient their reactive carbons next to N predominantly towards the Au. Due to their incommensurability with the Au(111) surface azafullerene islands display significant variations in the Au- $C_{59}N$ contact distance. We stress that the Au lattice mismatch imposes some tilting and lifting of fullerene cages directly seen in our STM images (Fig. 1c). According to the DFT calculations, such local contact variations tune the charge transfer between the substrate and $C_{59}N$ (section SA in supplementary information), yet they keep the nitrogen of the azafullerene cages oriented toward Au at ~ 30 deg from the (111) normal. This interacting contact layer of $C_{59}N$ monomers then serves as a buffer layer and a template for the growth of subsequent 2nd layer of $C_{59}N^{\bullet}$ radicals. In this 2nd layer, the coupling to the substrate is negligible as concluded from: (i) both C 1s and N 1s XPS binding energies reproduce those of a multilayer system and (ii) the lack of linear dichroism in N 1s NEXAFS spectra, which indicates that $C_{59}N$ are no longer orientationally locked and can now orient freely in space. Provided that the $C_{59}N$ filling of the 2nd layer is low as is the case for (10.5 Å–7.3 Å) and (11.5 Å–10.5 Å), these 2nd layer molecules remain mostly isolated monomers with highly expressed radical character. They are therefore recognized as a novel high spin-density phase. Upon further increase of the 2nd layer filling (approaching 2 ML as is the case for (17 Å–11.5 Å)) statistically, more and more azafullerenes in the second layer find themselves in next neighbor positions, where they are able to reorient and couple in $(C_{59}N)_2$ dimers. Upon dimerization they lose their radical character and the N 1s NEXAFS resonance at 400.5 eV disappears. The dimerization into non-magnetic $(C_{59}N)_2$ therefore starts as early as the 2nd layer approaches full completion.

Conclusions

In conclusion, we explored the sensitivity and high resolution of low-temperature STM and the XPS/NEXAFS spectroscopy supported by DFT computations to study the stability of $C_{59}N^{\bullet}$ radicals on Au(111) surface when deposited in vacuum by thermal sublimation. In the first monolayer of $C_{59}N$, adsorbed azafullerenes form a hexagonal lattice of monomers, where they retain their monomer character, but on average partially lose their radical character due to interaction with Au. Although the particular molecular orientation where the azafullerene carbon dangling bond directly faces a Au atom while at the same time the nitrogen orients towards the substrate at $30\pm 3^{\circ}$ average angle remains robust over the 1st monolayer, local variations in the Au- $C_{59}N$ distance result in the variations in the charge transfer between $C_{59}N$ and the substrate. Such first contact monolayer with non-uniform quenching of the radical state nevertheless serves as a passivating template layer for additional azafullerenes that are deposited on top. Isolated orientationally disordered $C_{59}N^{\bullet}$ monomers in the 2nd layer are uncoupled and fully retain their radical state. The sacrificial role of the 1st layer can then be exploited to form stable radical monomers in the second, non-contact layer. In-plane dimerization of the 2nd layer molecules only begins for higher coverages, on approaching the completion of the second layer.

The discovery of a supramonolayer phase of azafullerene monomers with expressed radical character on top of a passivating $C_{59}N$ monomer layer/Au(111) therefore demonstrates that spin active azafullerene radicals may be formed when weakly coupled to the substrate. Due to the extremely long coherence times of $C_{59}N^{\bullet}$ spin states,¹⁰ the possibility of having stable two-dimensional $C_{59}N^{\bullet}$ lattices may open intriguing opportunities for the coherent manipulation of molecular spin qubits. Moreover, the robustness of $C_{59}N^{\bullet}$ radical states for film thicknesses is important for the design of surface fullerene synthetic and catalytic processes. This simple approach of first forming a stable non-radical sacrificial layer before

subsequently depositing spin active molecules may also be applicable for other molecular radical systems.

Methods

(C₅₉N)₂ synthesis and characterization

Powder samples of azafullerene dimer (C₅₉N)₂ were synthesized following the standard procedure described in the literature.⁵ The sample purity was followed with the high-performance liquid chromatography (HPLC) where HPLC trace after recycling shows a single peak (Fig. S7). Next, (C₅₉N)₂ samples were characterised with ¹³C nuclear magnetic resonance (NMR) in deuterated ortho-dichlorobenzene. The ¹³C NMR spectrum (Fig. S8) shows a number of sharp peaks in the range between 136.4 ppm and 148.7 ppm and separated peaks at 155.8 ppm and 125.1 ppm, all of them due to *sp*² carbons. The separated peak at 108.0 ppm is due to the inter-azafullerene bonding carbon sites with carbon orbitals close to *sp*³. All these peaks are fingerprints of (C₅₉N)₂ and are in full agreement with the data reported in the literature²⁵ and at the same time confirm high purity of our samples.

Low-temperature scanning tunneling microscopy

Prior to deposition and low-temperature STM measurements, special care was taken to thoroughly clean the Au(111) surface and the azafullerene sample material. Au(111) surface was cleaned using the standard Ar⁺ sputtering (10 μA, 1kV) and annealing (up to 800K) cycles until a clean and well-ordered surface showing Herringbone reconstruction was obtained. The azafullerene molecules were deposited from a (C₅₉N)₂ powder using a homemade evaporator, consisting of a quartz tube with a tungsten filament wrapped around it. Due to the design of the evaporator, it was not possible to reliably measure its temperature during deposition. Thus, to ensure good reproducibility, the heating current was used as a measure of the evaporation

rate. First, the molecules were degassed for several days at 1.6 A in UHV. For each deposition the current was ramped over the course of several hours to 4.0 A, keeping the pressure in the evaporation chamber in 10^{-10} mbar range.

After the deposition, the samples were immediately transferred to the Specs low-temperature JT-STM with a base temperature of 4.2 K. Measurements were performed using electrochemically etched W tips, reconditioned in-situ by controlled tip-sample interaction and characterized on a clean Au(111) or Ag(111) surface. Topography images were taken in constant current mode ($I = 10\text{-}200$ pA). At negative bias voltages electrons dominantly tunnel from the sample into the tip, allowing us to image occupied states while using positive bias voltages probes the unoccupied states of the sample. In order to precisely determine intermolecular distances the microscope calibration was verified using known herringbone reconstruction parameters.

XPS and NEXAFS spectroscopy

The XPS and NEXAFS measurements were performed at the ALOISA beamline of the Elettra Synchrotron Facility, Trieste.²⁶ The Au(111) substrate surface was cleaned by repeated cycles of sputtering (1.5 kV Ar⁺) and annealing up to 723 K. The (C₅₉N)₂ was sublimed from a homemade boron nitride crucible, at a starting temperature of 670 K, up to 830 K; the increase in the sublimation temperature in order to deposit the same amount of material is possibly due to C₅₉N polymerization reactions inside the crucible. The overall film thickness of the deposited C₅₉N has been determined from the intensity attenuation of the Au 4f peak due to inelastic scattering of photoelectrons passing through the organic overlayer.²⁷ Core level photoemission data were acquired in normal emission geometry with a constant 4° grazing angle of linearly p-polarized light beam with respect to the Au(111) surface plane. The C 1s and N 1s XPS spectra were acquired at a photon energy of 515 eV with a total energy resolution

of 160 meV. Binding energies were calibrated with respect to the bulk spectral component of the Au 4f_{7/2} peak at 84.0 eV.²⁸ C-K edge and N-K edge NEXAFS spectra were acquired in partial electron yield mode by means of a channeltron multiplier equipped with a negatively biased grid to filter out low energy secondary electrons, in order to improve the signal to background ratio. In order to investigate the sample linear dichroism, the NEXAFS spectra were acquired at two different orientations of the synchrotron beam with respect to the surface plane, namely transverse magnetic (p-polarization) and transverse electric (s-polarization) geometry, by sample rotation around the photon beam axis. The beam grazing angle was kept constant at 6°. The photon energy calibration and photon flux normalization methods are described in detail elsewhere.²⁹ Both XPS and NEXAFS measurements were carried out with the sample temperatures between 300 K and 430 K.

DFT calculations

Ground-state density functional (DFT) calculations were carried out using the AIMPRO code^{30–32} using the local density approximation for exchange-correlation energy.³³ Kohn–Sham wave functions for C and N are constructed using localized Gaussian orbital functions multiplied by polynomials, with 38 and 40 independent functions respectively ($l \leq 2$), with plane-wave energy cut-off of 175 Ha. Calculations were spin optimized and polarized with different integer spin states tested (only the most stable are reported here). Relativistic pseudopotentials given by Hartwigsen, Goedecker, and Hutter (HGH)³⁴ with a finite electron Fermi temperature of $kT = 0.001$ eV were utilized. Systems were geometrically converged within $10^{-5} a_B$ in position (here a_B is Bohr radius) and 10^{-6} Ha in energy. To investigate angle-energy dependency of the adsorbed C₅₉N, single point energy calculations were carried changing only the angle of the C₅₉N molecule with respect to its center of mass, without letting

any atoms relax (i.e., optimize their positions). This constraint is imposed in order to avoid unintended cage movement.

For the hybrid system calculations, 2x2 supercell Au₃₆ triple-layer Au(111) slabs were created in hexagonal supercells, allowing atoms and lattice parameter to vary with a 6x6x1 k-point mesh, until reaching convergence ($a_0 = 9.72 \text{ \AA}$). A cell c-axis spacing of $>26 \text{ \AA}$ is chosen and fixed, to ensure there is no interaction between C₅₉N• and the base of the neighboring slab. The C₅₉N spacing is essentially imposed by the choice of supercell, and as such should not be compared directly to the experimental STM spacing. A single C₅₉N was added in close-packed direction oriented along [1-10] on the unreconstructed Au(111) trilayer (9.72 \AA C₅₉N spacing, i.e. 1 C₅₉N per 2x2 Au supercell), all atoms allowed to fully relax, with lattice parameters fixed. Once converged, the C₅₉N was then rotated about its centre of mass in steps of 5°/10°, and single point energy calculations were performed to explore the energy barrier for molecular rotation. Azafullerene charge state was determined through Mulliken population analysis.

To model the 2ML system, a radical C₅₉N• was added on top of the first monolayer with the radical facing towards the Au layer. We assume AB azafullerene stacking and a cell c-axis spacing increase to $>32 \text{ \AA}$. All atoms were allowed to relax. To explore the effects of coverage density, a 144 atoms 4x4 Au supercell was created, where a single C₅₉N• was added on it (25% coverage), as well as (C₅₉N)₂ for a 50% coverage. All atoms were again relaxed with a 3x3x1 k-point mesh.

NEXAFS spectra for C₅₉N⁺, C₅₉N•, C₅₉N⁻, and (C₅₉N)₂ were calculated using the ORCA code^{35,36} within a hybrid time-dependent DFT framework (TD-DFT). The hybrid TDDFT calculations were carried out at B3LYP³⁷ / ZORA-def2-TZVP³⁸⁻⁴⁰ level with def2/J auxiliary basis set, spin-unrestricted SCF and RIJCOSX approximation, after DFT geometry optimization and frequency calculations at B3LYP / 6-31G**⁴¹⁻⁴⁶ level. The default setting

was used for the other parameters. For C₅₉N-Au₂ complex, def2-TZVP basis set was instead used for NEXAFS calculations.

Supporting Information Available:

Figure S1: STM image of C₅₉N island on Au(111) substrate and its cross-section analysis along 3 different directions.

Figure S2: DFT calculations of close-packed C₅₉N• monomers on Au(111).

Figure S3: Projected density of states (eV) for C₅₉N• on Au (111) at low surface density calculated by DFT.

Figure S4: C 1s shake-up spectrum of C₅₉N films on Au(111).

Figure S5: Polarization NEXAFS spectra of C 1s and N 1s at different layers of C₅₉N•.

Figure S6: Calculated N 1s NEXAFS spectra of artificial C₅₉N-Au₂ complex with different C-Au bond lengths.

Figure S7: HPLC trace of (C₅₉N)₂ sample.

Figure S8: Solution ¹³C NMR spectrum of as-prepared (C₅₉N)₂ sample.

Section SA: C₅₉N radical state within the 1st monolayer.

Figure S9: N 1s NEXAFS spectra for increasing C₅₉N coverage.

Figure S10: N 1s NEXAFS spectra of C₅₉N with different film thickness and after annealing.

Figure S11: Calculated bonding orbital and charge density plots of C₅₉N on Au substrate.

Figure S12: Plot of calculated total system spin as a function of Au-C distance.

Corresponding authors

Chris Ewels: chris.ewels@cnrs-imn.fr

Dean Cvetko: dean.cvetko@fmf.uni-lj.si

Denis Arčon: denis.arcon@ijs.si

Present Addresses

Y.T: Jožef Stefan Institute, Jamova 39, SI-1000, Ljubljana, Slovenia

Author contributions

YT, BA and CE performed DFT calculations; YT, MvMM, and EZ performed STM observation; YT, GK, LS, GB, LF, AM, DC and DA performed NEXAFS and XPS experiments; RCV, NT, and HAW synthesized and characterized C₅₉N. This work was conceived and developed by HAW, NT, CE, DC and DA. All authors contributed to the analysis and interpretation of the data and editing of the manuscript.

Acknowledgements

YT acknowledges financial supports by the Research Grant for Young Researchers (CAREM, Hokkaido University) and the Japanese “JSPS Overseas Research Fellowships” scheme, and HPC facilities of Faculty of mathematics and physics at the University of Ljubljana. GK acknowledges financial support from the Slovenian Research Agency through research projects, grant numbers J1-3007 and J2-2514. DC and GK acknowledge financial support from the Slovenian Research Agency through research program, grant number P1-0112. BA acknowledges financial support by the EUR LUMOMAT project and the Investments for the Future ANR-18-EURE-0012. DA acknowledges financial support of Slovenian Research Agency through research program, grant number P1-0125, and through research projects, grant

numbers J1-3007 and N1-0220. CE and DA acknowledge the PHC Proteus Agreement 46151XJ and the Ministries of Europe and Foreign Affairs (MEAE) and Higher Education and Research (MESR) for exchange funding. EZ and MvMM acknowledges financial support of Slovenian Research Agency through research program, grant number P1-0099. YT, RCV, CE, NT and DA acknowledge COST Action CA21126 - Carbon molecular nanostructures in space (NanoSpace), supported by COST (European Cooperation in Science and Technology).

Abbreviations

ML, monolayer; XPS, X-ray photoemission spectroscopy; NEXAFS, X-ray absorption fine structure spectroscopy; STM, scanning tunneling microscopy; DFT, density functional theory; SUMO, singly unoccupied molecular orbital; UHV, ultra-high vacuum; HOMO, highest occupied molecular orbital; LUMO, lowest unoccupied molecular orbital; TDDFT, time-dependent density functional theory; SOMO, singly occupied molecular orbital.

References

1. Hicks, R. G. What's New in Stable Radical Chemistry? *Org. Biomol. Chem.* **2006**, *5*, 1321–1338. <https://doi.org/10.1039/B617142G>.
2. Gaita-Ariño, A.; Luis, F.; Hill, S.; Coronado, E. Molecular Spins for Quantum Computation. *Nat. Chem.* **2019**, *11*, 301–309. <https://doi.org/10.1038/s41557-019-0232-y>.
3. Hioe, J.; Zipse, H. Radical Stability and Its Role in Synthesis and Catalysis. *Org. Biomol. Chem.* **2010**, *8*, 3609–3617. <https://doi.org/10.1039/C004166A>.
4. Andreoni, W.; Gygi, F.; Parrinello, M. Impurity States in Doped Fullerenes: C₅₉B and C₅₉N. *Chem. Phys. Lett.* **1992**, *190*, 159–162. [https://doi.org/10.1016/0009-2614\(92\)85318-5](https://doi.org/10.1016/0009-2614(92)85318-5).

5. Hummelen, J. C.; Knight, B.; Pavlovich, J.; González, R.; Wudl, F. Isolation of the Heterofullerene C₅₉N as Its Dimer (C₅₉N)₂. *Science* **1995**, *269*, 1554–1556.
<https://doi.org/10.1126/science.269.5230.1554>.
6. Arčon, D.; Pregelj, M.; Cevc, P.; Rotas, G.; Pagona, G.; Tagmatarchis, N.; Ewels, C. Stability, Thermal Homolysis and Intermediate Phases of Solid Hydroazafullerene C₅₉HN. *Chem. Commun.* **2007**, *32*, 3386–3388. <https://doi.org/10.1039/B703766J>.
7. Hasharoni, K.; Bellavia-Lund, C.; Keshavarz-K, M.; Srdanov, G.; Wudl, F. Light-Induced ESR Studies of the Heterofullerene Dimers. *J. Am. Chem. Soc.* **1997**, *119*, 11128–11129. <https://doi.org/10.1021/ja972002y>.
8. Simon, F.; Arčon, D.; Tagmatarchis, N.; Garaj, S.; Forro, L.; Prassides, K. ESR Signal in Azafullerene (C₅₉N)₂ Induced by Thermal Homolysis. *J. Phys. Chem. A* **1999**, *103*, 6969–6971. <https://doi.org/10.1021/jp9912915>.
9. Gruss, A.; Dinse, K. P.; Hirsch, A.; Nuber, B.; Reuther, U. Photolysis of (C₅₉N)₂ Studied by Time-Resolved EPR. *J. Am. Chem. Soc.* **1997**, *119*, 8728–8729.
<https://doi.org/10.1021/ja971669h>.
10. Tanuma, Y.; Stergiou, A.; Bobnar, A. B.; Gaboardi, M.; Rio, J.; Volkmann, J.; Wegner, H. A.; Tagmatarchis, N.; Ewels, C.; Arcon, D. Robust Coherent Spin Centers from Stable Azafullerene Radicals Entrapped in Cycloparaphenylene Rings. *Nanoscale* **2021**, *13*, 19946–19955. <https://doi.org/10.1039/D1NR06393F>.
11. Stergiou, A.; Rio, J.; Griwatz, J. H.; Arčon, D.; Wegner, H. A.; Ewels, C. P.; Tagmatarchis, N. A Long-Lived Azafullerenyl Radical Stabilized by Supramolecular Shielding with a [10]Cycloparaphenylene. *Angew. Chem. Int. Ed.* **2019**, *58*, 17745–17750. <https://doi.org/10.1002/anie.201909126>.
12. Pinto, D.; Paone, D.; Kern, B.; Dierker, T.; Wiczorek, R.; Singha, A.; Dasari, D.; Finkler, A.; Harneit, W.; Wrachtrup, J.; Kern, K. Readout and Control of an

Endofullerene Electronic Spin. *Nat. Commun.* **2020**, *11*, 6405.

<https://doi.org/10.1038/s41467-020-20202-3>.

13. Schulte, K.; Wang, L.; Moriarty, P. J.; Prassides, K.; Tagmatarchis, N. Resonant Processes and Coulomb Interactions in $(C_{59}N)_2$. *J. Chem. Phys.* **2007**, *126*, 184707. <https://doi.org/10.1063/1.2730787>.
14. Butcher, M. J.; Jones, F. H.; Beton, P. H.; Moriarty, P.; Cotier, B. N.; Upward, M. D.; Prassides, K.; Kordatos, K.; Tagmatarchis, N.; Wudl, F.; Dhanak, V.; Johal, T. K.; Crotti, C.; Comicioli, C.; Ottaviani, C. $C_{59}N$ Monomers: Stabilization through Immobilization. *Phys. Rev. Lett.* **1999**, *83*, 3478–3481. <https://doi.org/10.1103/PhysRevLett.83.3478>.
15. Butcher, M. J.; Jones, F. H.; Cotier, B. N.; Taylor, M. D. R.; Moriarty, P.; Beton, P. H.; Prassides, K.; Tagmatarchis, N.; Comicioli, C.; Ottaviani, C.; Crotti, C. Chemisorption of Azafullerene on Silicon: Isolating $C_{59}N$ Monomers. *Mater. Sci. Eng. B* **2000**, *74*, 202–205. [https://doi.org/10.1016/S0921-5107\(99\)00562-0](https://doi.org/10.1016/S0921-5107(99)00562-0).
16. Jones, F. H.; Butcher, M. J.; Cotier, B. N.; Moriarty, P.; Beton, P. H.; Dhanak, V. R.; Prassides, K.; Kordatos, K.; Tagmatarchis, N.; Wudl, F. Oscillations in the Valence-Band Photoemission Spectrum of the Heterofullerene $C_{59}N$: A Photoelectron Interference Phenomenon. *Phys. Rev. B* **1999**, *59* (15), 9834–9837. <https://doi.org/10.1103/PhysRevB.59.9834>.
17. Silien, C.; Marenne, I.; Auerhammer, J.; Tagmatarchis, N.; Prassides, K.; Thiry, P. A.; Rudolf, P. Adsorption of Fullerene and Azafullerene on Cu(111) Studied by Electron Energy Loss Spectroscopy. *Surf. Sci.* **2001**, *482–485*, 1–8. [https://doi.org/10.1016/S0039-6028\(00\)01000-1](https://doi.org/10.1016/S0039-6028(00)01000-1).
18. Low, J. Z.; Kladnik, G.; Patera, L. L.; Sokolov, S.; Lovat, G.; Kumarasamy, E.; Repp, J.; Campos, L. M.; Cvetko, D.; Morgante, A.; Venkataraman, L. The Environment-

- Dependent Behavior of the Blatter Radical at the Metal–Molecule Interface. *Nano Lett.* **2019**, *19*, 2543–2548. <https://doi.org/10.1021/acs.nanolett.9b00275>.
19. Patera, L. L.; Sokolov, S.; Low, J. Z.; Campos, L. M.; Venkataraman, L.; Repp, J. Resolving the Unpaired-Electron Orbital Distribution in a Stable Organic Radical by Kondo Resonance Mapping. *Angew. Chem. Int. Ed.* **2019**, *58*, 11063–11067. <https://doi.org/10.1002/anie.201904851>.
 20. Brown, C. M.; Cristofolini, L.; Kordatos, K.; Prassides, K.; Bellavia, C.; González, R.; Keshavarz-K., M.; Wudl, F.; Cheetham, A. K.; Zhang, J. P.; Andreoni, W.; Curioni, A.; Fitch, A. N.; Pattison, P. On the Crystal Structure of Azafullerene (C₅₉N)₂. *Chem. Mater.* **1996**, *8*, 2548–2550. <https://doi.org/10.1021/cm960354i>.
 21. Paßens, M.; Karthäuser, S. Interfacial and Intermolecular Interactions Determining the Rotational Orientation of C₆₀ Adsorbed on Au(111). *Surf. Sci.* **2015**, *642*, 11–15. <https://doi.org/10.1016/j.susc.2015.07.025>.
 22. Pichler, T.; Knupfer, M.; Golden, M. S.; Haffner, S.; Friedlein, R.; Fink, J.; Andreoni, W.; Curioni, A.; Keshavarz-K., M.; Bellavia-Lund, C.; Sastre, A.; Hummelen, J.-C.; Wudl, F. On-Ball Doping of Fullerenes: The Electronic Structure of C₅₉N Dimers from Experiment and Theory. *Phys. Rev. Lett.* **1997**, *78*, 4249–4252. <https://doi.org/10.1103/PhysRevLett.78.4249>.
 23. Deng, Y.; Gao, B.; Deng, M.; Luo, Y. A Comparative Theoretical Study on Core-Hole Excitation Spectra of Azafullerene and Its Derivatives. *J. Chem. Phys.* **2014**, *140*, 124304. <https://doi.org/10.1063/1.4868717>.
 24. Schulte, K.; Wang, L.; Prassides, K.; Tagmatarchis, N.; Moriarty, P. J. C 1s Photoemission and Shake-up Features of (C₅₉N)₂. *J. Phys. Conf. Ser.* **2008**, *100*, 072024. <https://doi.org/10.1088/1742-6596/100/7/072024>.

25. Bühl, M.; Curioni, A.; Andreoni, W. Chemical Shifts of Diamagnetic Azafullerenes: (C₅₉N)₂ and C₅₉HN. *Chem. Phys. Lett.* **1997**, *274*, 231–234.
[https://doi.org/10.1016/S0009-2614\(97\)00676-3](https://doi.org/10.1016/S0009-2614(97)00676-3).
26. Floreano, L.; Naletto, G.; Cvetko, D.; Gotter, R.; Malvezzi, M.; Marassi, L.; Morgante, A.; Santaniello, A.; Verdini, A.; Tommasini, F.; Tondello, G. Performance of the Grating-Crystal Monochromator of the ALOISA Beamline at the Elettra Synchrotron. *Rev. Sci. Instrum.* **1999**, *70*, 3855–3864. <https://doi.org/10.1063/1.1150001>.
27. Cumpson, P. J.; Seah, M. P. Elastic Scattering Corrections in AES and XPS. II. Estimating Attenuation Lengths and Conditions Required for Their Valid Use in Overlayer/Substrate Experiments. *Surf. Interface Anal.* **1997**, *25*, 430–446.
[https://doi.org/10.1002/\(SICI\)1096-9918\(199706\)25:6<430::AID-SIA254>3.0.CO;2-7](https://doi.org/10.1002/(SICI)1096-9918(199706)25:6<430::AID-SIA254>3.0.CO;2-7).
28. Cossaro, A.; Floreano, L.; Verdini, A.; Casalis, L.; Morgante, A. Comment on “Local Methylthiolate Adsorption Geometry on Au(111) from Photoemission Core-Level Shifts”. *Phys. Rev. Lett.* **2009**, *103*, 119601.
<https://doi.org/10.1103/PhysRevLett.103.119601>.
29. Floreano, L.; Cossaro, A.; Gotter, R.; Verdini, A.; Bavdek, G.; Evangelista, F.; Ruocco, A.; Morgante, A.; Cvetko, D. Periodic Arrays of Cu-Phthalocyanine Chains on Au(110). *J. Phys. Chem. C* **2008**, *112*, 10794–10802. <https://doi.org/10.1021/jp711140e>.
30. Briddon, P. R.; Jones, R. LDA Calculations Using a Basis of Gaussian Orbitals. *Phys. Status Solidi B* **2000**, *217*, 131–171. [https://doi.org/10.1002/\(SICI\)1521-3951\(200001\)217:1<131::AID-PSSB131>3.0.CO;2-M](https://doi.org/10.1002/(SICI)1521-3951(200001)217:1<131::AID-PSSB131>3.0.CO;2-M).
31. Rayson, M. J. Rapid Filtration Algorithm to Construct a Minimal Basis on the Fly from a Primitive Gaussian Basis. *Comput. Phys. Commun.* **2010**, *181*, 1051–1056.
<https://doi.org/10.1016/j.cpc.2010.02.012>.

32. Briddon, P. R.; Rayson, M. J. Accurate Kohn–Sham DFT with the Speed of Tight Binding: Current Techniques and Future Directions in Materials Modelling. *Phys. Status Solidi B* **2011**, *248*, 1309–1318. <https://doi.org/10.1002/pssb.201046147>.
33. Grimme, S. Semiempirical GGA-Type Density Functional Constructed with a Long-Range Dispersion Correction. *J. Comput. Chem.* **2006**, *27*, 1787–1799. <https://doi.org/10.1002/jcc.20495>.
34. Hartwigsen, C.; Goedecker, S.; Hutter, J. Relativistic Separable Dual-Space Gaussian Pseudopotentials from H to Rn. *Phys. Rev. B* **1998**, *58*, 3641–3662. <https://doi.org/10.1103/PhysRevB.58.3641>.
35. Neese, F. The ORCA Program System. *WIREs Comput. Mol. Sci.* **2012**, *2*, 73–78. <https://doi.org/10.1002/wcms.81>.
36. Neese, F. Software Update: The ORCA Program System—Version 5.0. *WIREs Comput. Mol. Sci.* **2022**, *12*, e1606. <https://doi.org/10.1002/wcms.1606>.
37. Becke, A. D. Density-Functional Thermochemistry. III. The Role of Exact Exchange. *J. Chem. Phys.* **1993**, *98*, 5648–5652. <https://doi.org/10.1063/1.464913>.
38. Weigend, F.; Ahlrichs, R. Balanced Basis Sets of Split Valence, Triple Zeta Valence and Quadruple Zeta Valence Quality for H to Rn: Design and Assessment of Accuracy. *Phys. Chem. Chem. Phys.* **2005**, *7*, 3297–3305. <https://doi.org/10.1039/B508541A>.
39. Lenthe, E. van; Baerends, E. J.; Snijders, J. G. Relativistic Regular Two-Component Hamiltonians. *J. Chem. Phys.* **1993**, *99*, 4597–4610. <https://doi.org/10.1063/1.466059>.
40. van Wüllen, C. Molecular Density Functional Calculations in the Regular Relativistic Approximation: Method, Application to Coinage Metal Diatomics, Hydrides, Fluorides and Chlorides, and Comparison with First-Order Relativistic Calculations. *J. Chem. Phys.* **1998**, *109*, 392–399. <https://doi.org/10.1063/1.476576>.

41. Clark, T.; Chandrasekhar, J.; Spitznagel, G. W.; Schleyer, P. V. R. Efficient Diffuse Function-Augmented Basis Sets for Anion Calculations. III. The 3-21+G Basis Set for First-Row Elements, Li–F. *J. Comput. Chem.* **1983**, *4*, 294–301.
<https://doi.org/10.1002/jcc.540040303>.
42. Hariharan, P. C.; Pople, J. A. The Influence of Polarization Functions on Molecular Orbital Hydrogenation Energies. *Theor. Chim. Acta* **1973**, *28*, 213–222.
<https://doi.org/10.1007/BF00533485>.
43. Hehre, W. J.; Ditchfield, R.; Pople, J. A. Self—Consistent Molecular Orbital Methods. XII. Further Extensions of Gaussian—Type Basis Sets for Use in Molecular Orbital Studies of Organic Molecules. *J. Chem. Phys.* **2003**, *56*, 2257–2261.
<https://doi.org/10.1063/1.1677527>.
44. Pritchard, B. P.; Altarawy, D.; Didier, B.; Gibson, T. D.; Windus, T. L. New Basis Set Exchange: An Open, Up-to-Date Resource for the Molecular Sciences Community. *J. Chem. Inf. Model.* **2019**, *59*, 4814–4820. <https://doi.org/10.1021/acs.jcim.9b00725>.
45. Feller, D. The Role of Databases in Support of Computational Chemistry Calculations. *J. Comput. Chem.* **1996**, *17*, 1571–1586. [https://doi.org/10.1002/\(SICI\)1096-987X\(199610\)17:13<1571::AID-JCC9>3.0.CO;2-P](https://doi.org/10.1002/(SICI)1096-987X(199610)17:13<1571::AID-JCC9>3.0.CO;2-P).
46. Schuchardt, K. L.; Didier, B. T.; Elsethagen, T.; Sun, L.; Gurumoorthi, V.; Chase, J.; Li, J.; Windus, T. L. Basis Set Exchange: A Community Database for Computational Sciences. *J. Chem. Inf. Model.* **2007**, *47*, 1045–1052. <https://doi.org/10.1021/ci600510j>.